A numerical assessment of variable saturation of the upper layers on the ground borne vibrations from underground trains: a case history

Nicola Pontani*[a], Luca Martinelli[a], Marco Acquati[b], Cristina Jommi[a,c]

[a] *Department of Civil and Environmental Engineering, Politecnico di Milano, piazza Leonardo da Vinci 32, Milano, 20133, Italy*
[b] *MM S.p.A., via del Vecchio Politecnico 8, Milano, 20121, Italy*
[c] *Faculty of Civil Engineering and Geosciences, Stevinweg 1, Delft, 2628 CN, The Netherlands*

Abstract

Ground borne vibrations generated by the passage of underground trains may change over time due to objective causes, such as increasing weight and speed of trains or ageing of the infrastructure components, as well as a variation in the dynamic response of the soil surrounding the tunnel. Among the possible causes of changes in the soil dynamic response, its hydrologic state has been seldom investigated. In this contribution, the role played by the conditions of the soil above the water table is addressed, starting from a case history in the city of Milano. Two-dimensional plane strain numerical models have been developed for the infrastructure. The models were calibrated on the results of two geophysical investigations performed at the same site in the city centre, but at two different times, which allowed distinguishing different dynamic responses. The system was excited by a synthetic load time history, matching a reference dynamic load spectrum included in Italian recommendations. Limitations of using this input on a 2D plane strain model was assessed by comparing the computed vibrations with experimental acceleration records collected on the tunnel. The results of the two numerical models are compared with those of a simulation performed assuming fully dry conditions above the water table. Overall, the set of analyses shows that even small changes in the dynamic response of the soil, interpretated as a consequence of variable saturation, may result in a change of a few decibels in the acceleration levels. Much larger accelerations are predicted on average with the simpler dry model, clearly showing the advantages of a more

accurate modelling strategy.

Keywords: underground trains, ground borne vibrations, geophysical investigation, partial saturation, FE numerical analysis

*Corresponding author: nicola.pontani@polimi.it

---

1. Introduction

The passage of underground trains produces both noise and vibrations. The former is generally caused by structural vibrations due to interactions between the elements of the rail-wheel-carriage system [1]. The latter are mainly produced by track asperities, wheel irregularities, i.e. wheel flats, poor welds or spatial variation of the rail support stiffness, e.g. ballasted tracks [2, 3, 4]. The increasing weight and speed of trains together with the natural ageing of the railway track can be the cause of a growth of vibrations over the years. This fact is important in urban settings as it may dramatically affect the comfort of people occupying the buildings nearby the railway route.

Besides all the mentioned factors, the role played by a change in the dynamic response of the soil - tunnel system has to be considered. From this point of view, it is well known that the excitation produced by the passage of underground trains is affected by the geometry and material of the tunnel as well as the properties of the surrounding soils [5]. Nevertheless, small attention has been paid in the past on the interference of the water regime within the soil on the response of the infrastructure. As a matter of fact, the position of the water table, together with the conditions of partial saturation affecting the shallowest layers of soil, may produce variations in the vibrations induced by the passage of trains. Few contributions may be found in the literature regarding the influence of the position of the water table on the upper layer response [6, 7]. The results of a recent study on Milano historic metro lines [7] highlight an increase of vibrations when the aquifer is located below the track level. This configuration is particularly crucial for the tunnels of the M1 line. The presence of vertical diaphragm walls partially immersed in the lower aquifer may induce a box-like effect, trapping the energy transmitted by the train and returning it to the tunnel. As a result, the oscillation at the ground can be emphasised. Recently, Di et al. have addressed the influence of saturation over the water table by means of an analytical approach [8, 9].

The position of the water table and the water exchanges at the ground govern the profiles of degree of saturation and suction over depth, resulting in a change in the dynamic behaviour of the soil over time. In coarse grained soils, such as those characterising the Milano area, the shear modulus at small strains can vary with the decrease of degree of saturation or suction in a non-monotonic or monotonic way [10, 11, 12, 13]. Furthermore, experimental data show a dependence on the fabric [14] and drying - wetting episodes [15, 16], as well. For what concerns the damping ratio, an increase with the decrease of shear stiffness is generally observed [17, 18]. Geophysical tests, with special attention to the ones based on surface waves [19], may be used to directly assess the variation over time of density, stiffness and damping in soils undergoing variations in the degree of saturation. The use of this type of test is always recommended when dynamic soil-structure interaction problems are faced, as in the case presented herein. In addition, by taking advantage of the speed of execution, the results of multiple tests can be combined together overcoming some inevitable limitations of each separate technique [20].

To quantify possible changes in the dynamic behaviour of the soil along the Milano M1 metro line, Metropolitana Milanese (MM) has been performing a number of geophysical tests along it. One of these, conducted in March 2012, was repeated 9 years later, in April 2021. The comparison between the two tests highlights differences, which are interpreted as the consequence of different degree of saturation profiles in the two circumstances. To predict the change in the induced environmental vibration, the profile of the physical and mechanical quantities that arise from the two investigations is implemented in a 2D finite element model.

Several possibilities are available in the literature to model the dynamic response of the tunnel-soil system to underground train passage. Analytical or semi-analytical models are efficient tools, which are capable of providing low computational effort solutions. Nonetheless, they typically suit just particular situations. For instance, the Pip in Pip model [21] is a three-dimensional semi-analytical model that requires the absence of a free surface and a tunnel with a cylindrical cross-section. The majority of such models is conceived for single-phase or saturated porous media, although an analytical model for cylindrical tunnels in unsaturated homogeneous soils has been proposed recently [8]. The model has been extended to layered media [9], enriching the representation with a discontinuous variation of the degree of saturation over depth. For complex geometries, 3D finite element analyses

would be the optimal choice, however, at the expenses of a computational effort which may become too high to afford [22]. A possible alternative to cumbersome 3D models for longitudinally invariant structures is the use of 2.5D FE-BE models [23, 24]. This class of methods only requires a 2D spatial discretization of the tunnel and the surrounding soil. The Fourier transform of the longitudinal coordinate is then exploited to capture the spatial response of the system. Efforts have been done to extend available 2.5D FE-BE models to take care of the porous nature of saturated soils [25, 26] as well as to overcome the computational demand of the three dimensional model [27]. Plain strain finite element models have proved to be effective to preliminary address problems characterised by complex geometric configurations [28, 29]. A past study on the 2D and 3D response of cut-and-cover tunnels based on the FE - BE technique [30] has shown how 2D models typically overestimate the displacements induced at the ground surface and at the tunnel floor as a consequence of the smaller geometric damping compared to a fully 3D model. Comparisons between 2D and 2.5D finite/infinite elements method [31] led to the conclusion that the 2D plain strain soil response represents an upper bound also for 2.5D solutions. To the scope of this work, focused on the differences in the response due to different states of the same soil, a 2D approximation was considered acceptable, knowing that it will provide an upper bound to the response in the field.

In the models, the passage of a train is simulated in the time domain, applying a load time-history whose frequency content is generated by the load spectrum reported in the standard [32]. Special care has been taken in reproducing the frequency range which may generate discomfort to people, i.e 1 - 80 Hz [4, 33]. The numerical model reproduces a typical M1 line tunnel which is ideally surrounded by soils whose physical-mechanical properties and stratigraphic profile recall the area investigated in the 2012 and 2021 testing programs. The hydro-mechanical dynamic coupled analyses have been performed by means of the finite element code Tochnog [34].

Results are compared against a simpler numerical model. In the literature, it is generally suggested to model the soil as a mono-phase medium, given the impossibility of relative motion between pore water and solid skeleton for the frequency range typically interested by train vibrations, leading to an incompressible material if saturated conditions occurs, i.e. $\nu = 0.5$ below the water table [6, 35] and using dry conditions above it. This choice introduces a sharp contrast in terms of stiffness and acoustic impedance at the interface with the aquifer. This simplifying hypothesis is believed to

amplify the numerical estimate of the ground borne vibrations compared to the true ones. In this work, this hypothesis is removed, by better describing the smooth transition between saturated and unsaturated conditions in the upper soil layers.

The structure of the paper is as follows. First a description of the investigated area is given in terms of soil profile and groundwater regime before discussing the results of the geophysical tests. A picture of the main relevant characteristics of the M1 line in Milano is given, as well. Then the main numerical assumptions and details are presented. Finally, the results of the numerical study are discussed.

2. Case study

2.1. M1 metro line in Milan

The Metro line M1 is the first underground line built in Milano. The first section, opened on 1964 November 1, was constructed with a top-down sequence of excavations sustained by sheet piles. This method later became known as the "Metodo Milano" or "cut and cover". The Metro line M1 crosses the central part of the town at depths always smaller than 15.0 m [36], intersecting at times the piezometric surface of the first top aquifer, depending on the season. The tunnels, made of reinforced concrete, generally show two lateral diaphragm walls and a bottom inverted arch (Fig. 1). The railway track consists of wooden sleepers on ballast with standard rail gauge (Tab. 1). The general characteristics of a typical train ("Leonardo" cars) running on the line are reported in Tab. 2.

Rail gauge	m	1.435
Sleeper type	-	wood
Sleeper dimensions	m	2.6x0.16x0.24
Sleeper spacing	m	0.667
Ballast thickness	m	0.35

Table 1: General characteristics of Milano M1 line.

2.2. Site characterisation

To investigate the response of the layers transmitting the vibrations of the train line towards the surface, in the last decade Metropolitana Milanese

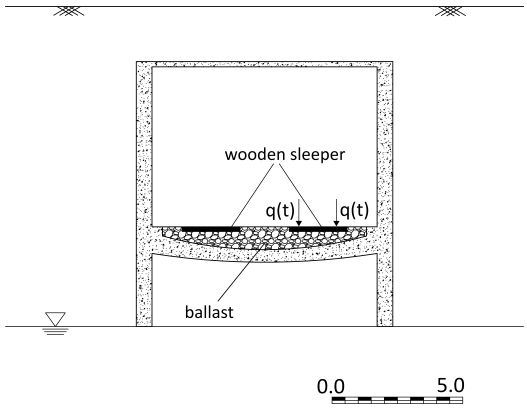

Figure 1: Reference cross section of the M1 metro line tunnel implemented in the models. The loads $q(t)$ represent the contact forces at the rails base.

Length	m	107.0
Width	m	2.85
Mass in service	kg	146800
Max speed	km/h	90
Car length	m	17.8
Boogies spacing	m	11.1
Wheels spacing	m	2.15
Axles per bogie	-	2
Bogies per coach	-	2
Number of coaches	-	6

Table 2: Technical features of Milano M1 line trains "Leonardo".

(MM) has been performing a number of geophysical - non invasive - investigations along it. One of them, performed in 2012 in the site illustrated in Fig. 2, was repeated in 2021 to asses possible variation over time of the dynamic response of the upper layers. Relevant information from the investigation is summarised in the following.

2.2.1. Grain size distribution and groundwater regime

The disturbed samples collected from surveys S1 and S2 (Fig. 2) give the grain size distribution profiles depicted in Fig. 3. As frequently encountered in the subsoil of Milano [36], a shallow layer of heterogeneous sandy silt overlies deposits characterised by higher contents of sand and gravel, which

Figure 2: Location of geophysical tests (highlighted area), surveys (S1 and S2) and piezometers (P1, P2, P3 and P4).

commonly extend to a depth of 40.0 m and host the shallowest aquifer of the town. The position of the water table inside this layer is strictly dependent on the water exchanges over the countryside north of Milano, obeying the hydrological cycle and anthropogenic demands [37]. In Fig. 4 the measurements of four piezometers report the temporal position of the water table around the area of interest. P1, the one closest to the investigations site, returns a water level of 102.8 m.a.s.l. in March 2012, when the tests have been performed. Being the ground surface at the site at 116.4 m.a.s.l., the depth of the water table at that time was 13.6 m. The increasing trend recorded by the piezometer between 2008 and 2014 may be interpreted as the most recent toe of an upward trend begun in the early 80's as a result of the closure of large industrial hubs located in the northern part of the town. Some difficulties arise in the identification of the water level in April 2021, when the second investigation campaign was performed, as measurements from P1 are not available. Three other piezometers close to the area report an opposite trend, showing a slight decrease of the water table in the period 2014 - 2018. Further information collected from the municipality of Milano indicates water table depths between 12 - 14 m for the area interest. In conclusion, even though the exact measure of the water level at the specific investigated site is not available in April 2021, it can be assumed that the water head was approximately coincident with the one measured in March 2012.

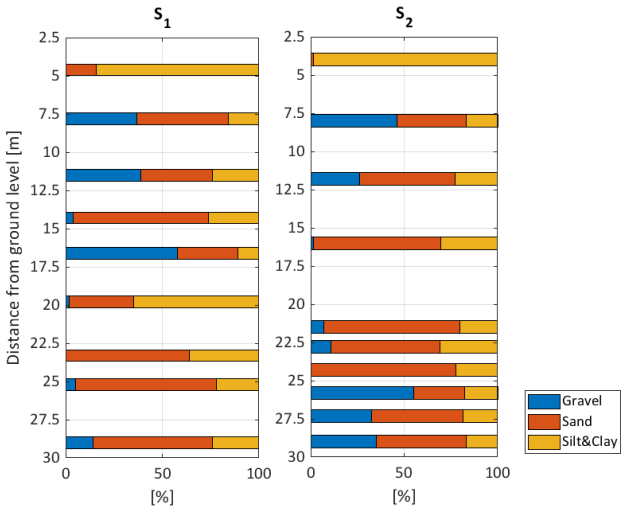

Figure 3: Grain size distribution from disturbed samples.

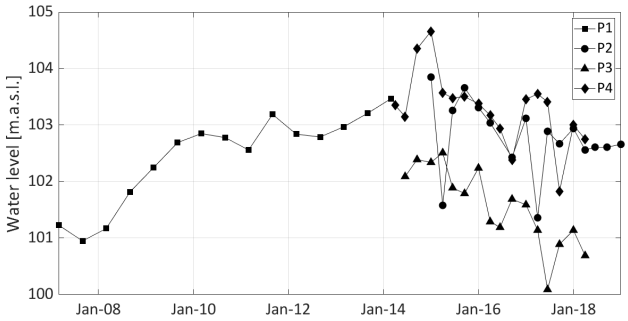

Figure 4: Water heads.

2.2.2. Geophysical test investigations

The results of the geophysical tests carried out in March 2012 and April 2021 are shown in Fig. 5. They consist in the profiles of the vertical component of shear and compression waves velocity, V_{SV} and V_P, density, ρ, Poisson's ratio, ν, Young modulus, shear stiffness and damping ratio at small strains, E, G and D. The derivation of the different quantities from the profiles of shear and compression waves and density followed the standard procedures adopted for visco-elastic media [38]. The results have been derived integrating data from the various geophysical techniques adopted on site, including seismic refraction tomography, Multichannel Analysis of Surface Waves (MASW), an improvement of the SASW technique [39], Refraction Microtremor (ReMi) [40] and the Horizontal-to-Vertical Spectral Ratio (HVSR) [41]. Both in 2012 and 2021, 24 geophones with a natural frequency of 4.5 Hz have been located along the 46.0 m long section S-S depicted in Fig. 2. For tomographies and MASW, the active source of seismic energy is provided by a 8 kg sledgehammer on a metal plate. DMT Compact and MAE X610S seismographs at 24-bit resolution were used in 2012 and 2021, respectively.

In Fig. 5 differences between the two profiles are evident, indicating a variation in the response of the same site over the period investigated. Moving from 2012 to 2021, an increment in both P waves velocity and density can be appreciated, resulting in a stiffer and less compressible soil, as highlighted by the profiles of the Young modulus, shear stiffness and Poisson's ratio. An opposite trend is shown by the damping ratio D, with lower values in 2021 than 2012 at depths greater than approximately 2.5 m. Minor variations affect the V_{SV} profiles. It is worthwhile observing that, even though geophysical tests provide a useful tool for the identification of the dynamic behaviour of soils at small strains, as they are often cheaper and less invasive than other techniques, they suffer to some extent from subjectivity in the interpretation of the data. However, the procedures used to derive the results in Fig. 5 starting from the data collected in the two years were kept identical to reduce the subjectivity in the comparison. Given the same experimental techniques used in the field and the same interpretation criteria adopted in the analysis of the data, the differences observed in the two profiles are deemed to be caused by changes in the environmental conditions occurred at the site between the two investigation time instants. The analysis of piezometric levels for the years 2012 and 2021 (Sec. 2.2.1) highlights no significant

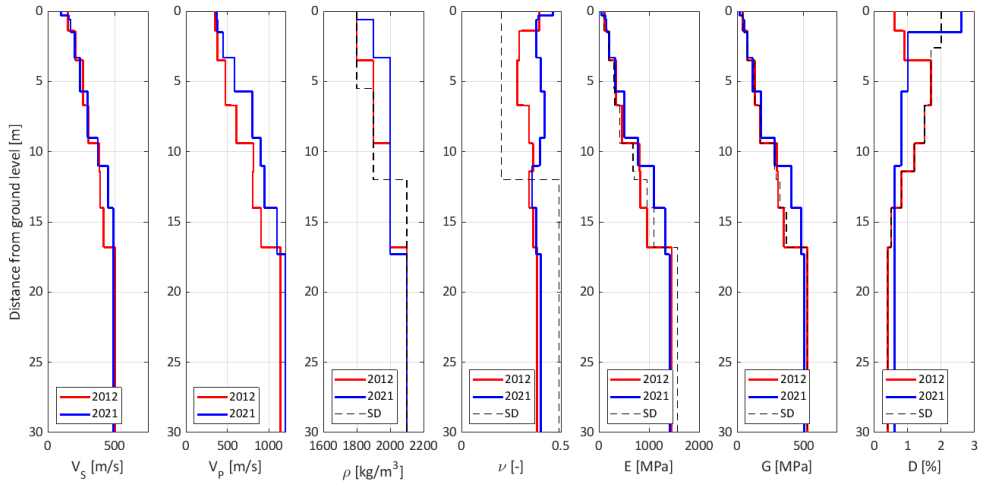

Figure 5: Results from geophysical tests (coloured solid lines) and SD scenario (black dashed lines).

variations in the position of the piezometric surface of the aquifer between the two moments. Therefore, the attention was focused on the shallowest portion of the investigated site, i.e., above the water table. The analysis of pluviometric data in the month before the two campaigns return a wetter period in April 2021 than in March 2012, being the total cumulative rainfall 47.8 mm and 18.2 mm in 2021 and 2012, respectively. As a result of the different cumulative rainfall, a different saturation profile is expected, which is assumed to be responsible for the measured differences in the response, affecting the unit weight, the effective confining pressure and, possibly, stiffness [38, 11] and damping [17]. When analysing the results, it can be appreciated that the largest differences are observed in the Poisson's ratio, hence, in the volumetric stiffness. This observation is coherent with a higher degree of saturation [10] of the upper portion of the soil profile over the first 10.0 m from the ground in 2021, following the higher cumulative rainfall. On the contrary, the difference in shear stiffness for the same change in the degree of saturation can hardly be appreciated. This can be due to the reduced resolution of the shear waves measurements compared to the small changes expected in a predominantly coarse grained soil [10]. Although the difference is very small, the drier the soil, the higher the shear stiffness at small strains, as expected [11, 14].

A remark on the reported damping ratio profiles must be added. Below

a depth of around 2.5 m, the less saturated state assumed for 2012 exhibits higher damping than the more saturated one in 2021. This is unexpected, since an increase in the energetic loss with the amount of water inside the pores is expected as a first approximation. Although very little data are available in the literature, the damping ratio is expected to follow the opposite trend compared to G with saturation. For coarse grained soils, with a significant percentage of gravel and poor retention properties, G shows a non-monotonic trend with a peak followed by a decrease at decreasing saturation [16]. It can be inferred that the opposite may be valid for damping, which could justify higher values at lower saturation. However, no studies have been found in the literature to prove this assumption and future experimental research is needed to clarify this aspect.

3. Numerical modelling

3.1. Balance equations and constitutive assumptions

Coupled hydro-mechanical dynamic analyses have been performed, based on the model described in the following. The dynamic fully-coupled soil-structure interaction problem is governed by the linear momentum and mass balance equations [34, 42]:

$$\nabla \cdot \boldsymbol{\sigma} - D\dot{\boldsymbol{u}} - \rho \boldsymbol{b} + \rho \ddot{\boldsymbol{u}} = \boldsymbol{0} \tag{1}$$

$$\nabla \cdot \boldsymbol{v} - \dot{\varepsilon}_v + \frac{1}{Q}\dot{u}_w = 0 \tag{2}$$

being $\boldsymbol{\sigma}$ the total stress tensor, $\dot{\boldsymbol{u}}$ and $\ddot{\boldsymbol{u}}$ the solid skeleton velocity and acceleration, $\boldsymbol{b}$ the body force density per unit mass, $\boldsymbol{v}$ the Darcy's seepage velocity, u_w the pore water pressure, D the damping coefficient, ρ the bulk density, $\dot{\varepsilon}_v$ the volumetric strain rate. For a single fluid phase, given the soil porosity, n, and the fluid bulk modulus, K_f, the storage coefficient Q^{-1} is:

$$\frac{1}{Q} = \frac{n}{K_f} \tag{3}$$

Below the piezometric surface K_f has been assummed equal to 2.2 GPa. Above, K_f decreases drammatically at decreasing saturation. The previous equations are valid under the assumptions of small strains and incompressible solid grains. In the following, the relative acceleration of the liquid phase with

respect to the solid one is neglected [42] and the pore gaseous phase pressure is assumed to be zero.

The strong formulation of the problem is completed with the constitutive equations. In case of linear elastic isotropic media, the fourth-order stiffness tensor can be defined in terms of Lamé constants as:

$$\boldsymbol{D} = 2G\mathbb{I} + \lambda \boldsymbol{I} \otimes \boldsymbol{I} \tag{4}$$

where $\lambda = 2G\nu/(1-\nu)$, being G the shear modulus at small strains and ν the Poisson's ratio. $\mathbb{I}$ and $\boldsymbol{I}$ are the fourth and second order identity tensors respectively. In the absence of in-situ measurements of the saturation degree and suction profiles, a direct insight on G and ν may be provided by the geophysical test results, on which they can be calibrated. As anticipated, the differences observed between 2012 and 2021 are assumed to come from different saturation profiles. The hydraulic conductivity was assigned based on available in-situ test results, which gave an average value of $k = 2.5 \cdot 10^{-4}$ m/s for an average porosity $n = 0.4$.

3.2. Geometry and materials

The profiles retrieved from geophysical tests were implemented in a two-dimensional finite element model with the aim to reproduce a tunnel cross-section (Fig. 6) subjected to a train passage. The location and geometry of the tunnel replicates the M1 Milan metro line (Sec. 2.1). The water table is assumed to be located at a depth of 12.1 m from the ground, at the base of the tunnel walls. This assumption is inconsistent with the data reproduced in Sec. 2.2.1. However, previous studies ([7]) has shown that this water table - tunnel combination should represent the worst scenario in terms of induced environmental vibrations. All the materials are modelled as linear elastic media with Rayleigh viscous damping, defined as [34]:

$$D = \alpha\rho + \beta E \tag{5}$$

being α and β the mass and stiffness proportional terms, calibrated on the profiles depicted in Fig. 5. The physical-mechanical properties of the concrete and the railway track were assigned on the basis of technical regulations and standards [43, 44], information from previous studies [4] and indications from MM. For the tunnel concrete, density, elastic modulus and Poisson's ratio were adopted as 2.5 Mg/m3, $2.5 \cdot 10^4$ MPa and 0.2, respectively. For

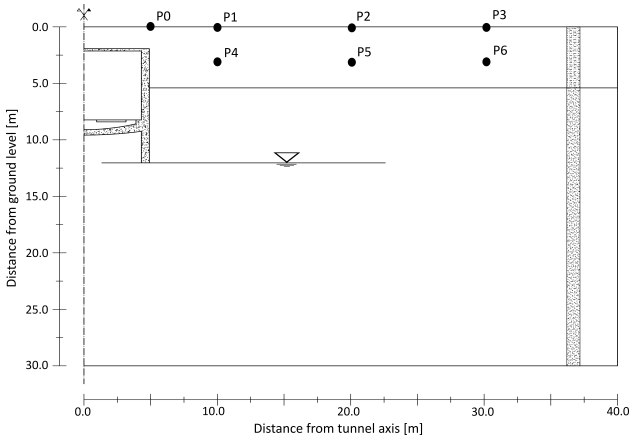

Figure 6: Dimensions of the reference M1-line cross section implemented in the numerical models. The water table is located at the base of the walls. The double-layer stratigraphy is implemented in the Saturated - Dry (SD) model. Station points, P_i, for results post-processing are represented, as well.

the ballast and wooden sleepers the same quantities are set to 1.3 and 1.0 Mg/m^3, $3.0 \cdot 10^2$ and $9.4 \cdot 10^2$ MPa, 0.3 and 0.1.

Following the approach suggested by Schevenels et al. (2004) [6], a third numerical model, named "SD" for Saturated-Dry, has been implemented. The soil above the water table is considered as dry, while the one below behaves as an incompressible, mono-phase medium. This model is built on the simplified double-layered stratigraphy derived from Fig. 3 and depicted in Fig. 6. The shallower silty sand layer has a dry density of 1.8 Mg/m^3, while the deeper one, a gravelly sand, is characterised by a density of 1.9 Mg/m^3 and 2.1 Mg/m^3 under dry and saturated conditions respectively. The Poisson's ratio ranges from 0.2 above the water table to 0.49 below. Assuming as a reference the shear wave velocities from the 2012 scenario, a new distribution for the shear stiffness and Young modulus is derived. All the profiles are represented in Fig. 5 by dashed lines.

3.2.1. Finite Element Simulations

The three models are made up of 21245 4-nodes isoparametric elements. The unstructured spatial discretisation of the domain is characterised by a denser square area of side 10.0 m all around the tunnel (Fig. 7), which is made up of elements of size $h_e = 0.2$ m. The right-hand sleeper at the tunnel floor, where the vertical loads are enforced, is discretized by finer elements

of dimensions 0.1. m, to allow proper transmission of the entire frequency content. The remaining part of the domain was discretized with elements of size 0.5 m on average. The dimension of elements has been fixed from preliminary analyses as a trade-off between the maximum transmissible frequency, i.e. 250 Hz, and computational time. In the preliminary simulations, not presented here, the upper bound for the elements dimension was set to [45] $h_{e,max} = \lambda_{min}/n_{nw}$, where n_{nw} is the required number of nodes to reproduce the wavelength $\lambda_{min} = V_S/f_{max}$. The highest frequency of the input load is $f_{max} = 250$ Hz, while $n_{nw} = 5$ is considered a reasonable choice. Since the velocity of shear waves increases over depth (Sec. 2.2.2), the size of the elements was varied between 0.1 m at the top and 0.4 m at the bottom of the model. Drained simulations were launched, taking 12 hours on a Dell Alienware computer with a 16-Core AMD Ryzen 9 5950X processor and a 128 GB RAM. As the energetic content of the computed signals in the soil (Fig. 6) was dampened out for frequencies greater than 100 Hz, the decision to increase the element size outside the volume depicted in Fig. 7 was taken, allowing a significant reduction in the calculation time. The extent of the domain (80x30 m) is determined in order to provide an accurate spatial overview on the propagation of the motion induced by the passage of the train. At the boundaries viscous damping conditions are implemented to guarantee the absence of reflections [46]. Damping coefficients along the normal and tangential directions (Fig. 8), C_N and C_T, are automatically calculated from adjacent elements as [34]:

$$C_N = \rho\sqrt{\frac{E}{\rho}\frac{1-\nu}{(1+\nu)(1-2\nu)}}, \quad C_T = \rho\sqrt{\frac{G}{\rho}} \tag{6}$$

Displacements and velocities cannot be enforced to be zero if dampers are present at the boundaries. Therefore, normal springs should be implemented. The stiffness of the springs was set to 10^7 MPa in order to avoid appreciable displacements in the initialization stage of the model.

After gravity is switched on in a quasi - static, drained step, springs are frozen so that all further stress changes can be dampened out.

3.2.2. Modelling the train passage

The passage of the train is modelled in the time domain enforcing a vertical load history at the rail - sleeper contact (Fig. 1). Following an approach similar to [47], the load is obtained from the combination of a static

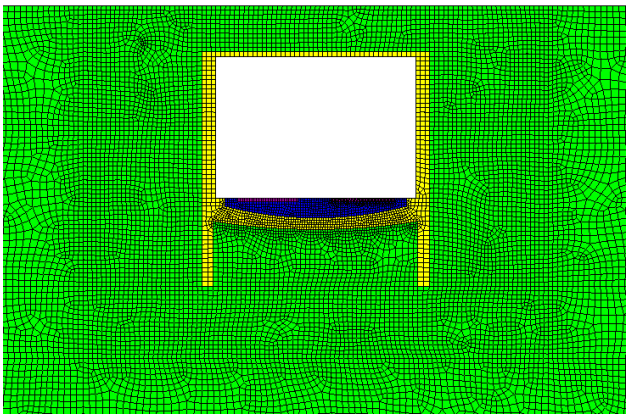

Figure 7: Detail of the adopted spatial discretization around the tunnel and modelled materials.

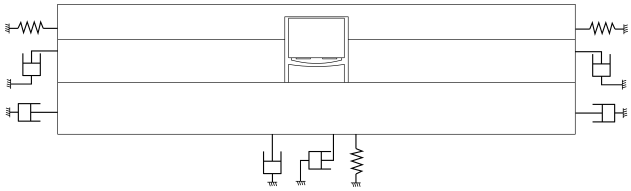

Figure 8: Boundary conditions implemented in the numerical models.

component, i.e. the total weight of the train, with a dynamic contribution:

$$q(t) = q_s + q_d(t) \tag{7}$$

with

$$q_s = \frac{Q_s N_{AB} N_{BC} N_C}{2BL} \tag{8}$$

where Q_s is the static axle load, N_{AB}, N_{BC}, N_C and L are the numbers of axles per bogie, bogies per coach, coaches and train length (Tab. 1 and Tab. 2) and $B = 0.15$ m is the width of the rail at the base. This approach reasonably agrees with the results of a previous study [27]. The authors, exploiting a 2.5D approach, find that for a velocity of the train below the speed of the Rayleigh wave in the soil, the dynamic response of the tunnel and the ground to quasi-static load is itself quasi-static. Therefore, the displacements suffered in the longitudinal direction by the tunnel tends to be uniform over the length of the train, with the exception of the ends. Consequently, the hypothesis of plane strain can be considered acceptable as a first approximation. Finally, the presence of rail pads in between rails and sleepers is disregarded as previous studies suggested poor influence of their stiffness on the frequency content transmitted beneath [4]. The second component, $q_d(t)$, is related to dynamic train-track interactions, which depend on the type of train and rail as well as on wheel-track unevenness and spatial variation of the support stiffness [3]. In the absence of specific information on the train-track system, the dynamic contribution to the total load is derived from the non-dimensional load spectrum, ε, provided by [32] in twelfths of octaves bands (Fig. 9) and defined as:

$$\varepsilon(f_j) = \frac{Q_d(f_j)}{Q_s} \tag{9}$$

being f_j the central frequency of the j-th band measured in Hz. The spectrum refers to a train with a static axle load $Q_S = 160.0$ kN, moving through a single-track tunnel at constant speed between 50.0 km/h and 60.0 km/h. The ballast is 0.35 m thick and the spacing between the sleepers is 0.6 m. These features replicate the general characteristics of the M1 line (Tab. 1 and Tab. 2). In the absence of details such as the length of signals and the sampling frequency used for the derivation of Eq. 9, an estimation of the power spectral density associated to each band, Δf_j, can be provided as:

$$W(f_j) = \frac{Q_d^2}{\Delta f_j} \tag{10}$$

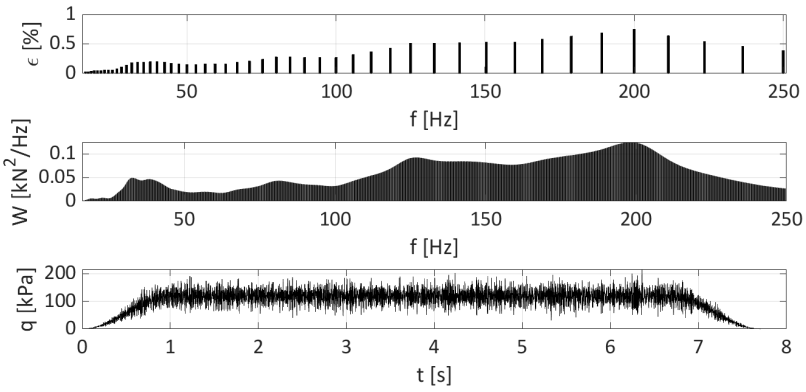

Figure 9: Non-dimensional dynamic load spectrum [32], estimated power spectral density and time-history of the enforced load (see Fig. 1)

.

An interpolation between the central band values is used to obtain a continuous representation of the power spectral density as depicted in Fig. 9. Assuming the process to be random and stationary [48], the amplitudes can be estimated as:

$$A_k = \sqrt{2W(f_k)\Delta f} \tag{11}$$

where $\Delta f = 0.01$ Hz is the frequency resolution, resulting from a simulated signal length of 100 s. Each frequency is associated with a uniformly distributed random phase, Φ_k, varying between 0 and 2π. Therefore, a complex amplitude spectrum can be obtained as:

$$a_k = A_k cos(\Phi_k), b_k = A_k sen(\Phi_k) \tag{12}$$

being a_k and b_k the components of a complex number $z_k = a_k + ib_k$ with $i = \sqrt{-1}$. The Inverse Fourier Transform of this spectrum results in a realisation of the load time-history. Considering the time spent by the train to cross the section at constant speed of 50.0 km/h, a length of 7.7 s is cut. Ramps are added at the ends to represent the arrival and removal of the train from the section, i.e. giving a non-stationary artificial trend to the process [48]. Their lengths have been arbitrarily set to 1.025 s. The final load history used for the simulation is represented in Fig 9.

4. Results

In this section, results from simulations for models from 2012 and 2021 geophysical tests are presented. The main differences are highlighted and comparisons with the "saturated-dry" scenario, SD, are provided.
Time-histories and Fourier amplitude spectra of the vertical and horizontal accelerations for control points P1, P2, P3, P4, P5 and P6 of Fig. 6 are represented in Figs. 10 - 13. At increasing distances from the tunnel, the amplitudes of the computed signals progressively decrease, as a consequence of geometrical attenuation and material damping [38]. The shift of the energetic content towards low frequencies, i.e. smaller than 50 Hz, shows a higher rate further away from the ground surface, i.e. points P4, P5 and P6, suggesting a different propagation mechanism with depth. The transition from a volume-wave driven mechanism to a surface wave one together with the vibratory motion of the tunnel ceiling, may explain the general growth of oscillations moving from -3.0 m depth to the ground level. For vertical accelerations, this happens in the frequency range 30-50 Hz at a distance of 5.0 m from the wall at the right hand side of the tunnel, i.e. P1 and P4, for all the considered scenarios. In P2 and P5, 2012 and SD show similar trend. Instead, the higher damping on surface for 2021 produces a less significant growth. At 25 m from the tunnel wall, i.e., P3 and P6, the energetic content of the signals between 20 - 40 Hz still remains significant. The horizontal components show a more uniform growth for frequencies smaller than 40 Hz at decreasing depths. The various scenarios overall return similar trends, with the exceptions of P5 and P3. In the former, the SD case emphasises frequencies between 30-40 Hz. In the latter, 2012 and 2021 return signals characterised by a significant energetic content in the range of frequency 20-40 Hz.

Different quantities may also be introduced to provide a synthetic picture of the induced vibrations. Two of them are the Root Mean Square (RMS) and the Peak Ground Acceleration (PGA), defined as [49]:

$$RMS = \sqrt{\frac{1}{T}\int_0^T a(t)^2} \tag{13}$$

and

$$PGA = max|a(t)| \tag{14}$$

being $a(t)$ the computed acceleration signal of length $T = 9.0$ s. A spatial view of the induced vibrations in terms of RMS and PGA is provided by

Fig. 14 for points lying at the ground, i.e. P0, P1, P2 and P3, and by Fig. 15 for those at a depth of 3.0 m from the ground, i.e. P4, P5 and P6. At the ground surface (Fig. 14) as a consequence of material and geometric damping, both RMS and PGA of the vertical accelerations decrease at increasing distances from the tunnel. The rate of decrease is higher in the neighborhood of the right wall, i.e. in the first 5.0 m along the path from P0 to P1, ranging from the 0.5% m/s^2/m, 0.6% m/s^2/m and 0.7% m/s^2/m for SD, 2012 and 2021 cases respectively and then becoming 0.17%m/s^2/m, 0.10% m/s^2/m and 0.070% m/s^2/m for the second 10.0 m, i.e. P1 - P2, and 0.11% m/s^2/m, 0.03% m/s^2/m and 0.034% m/s^2/m for the third ones, i.e. P2 - P3, for SD, 2012 and 2021 cases respectively. The vertical RMS predicted with the SD scenario are higher than the 2012 and 2021 everywhere, producing increments of 120.1%, 215.8% and 200% of the values predicted with the 2021 case. Variations are clear even between the 2012 and 2021 case as the former produces higher oscillations than the latter everywhere. Nonetheless, the predicted trends for the horizontal RMS and PGA present some differences compared to their vertical counterparts. While both 2012 and 2021 show a monotonic decreasing trend from the tunnel wall, SD reproduces a non-monotonic one. As a consequence, horizontal accelerations may be underestimated in the vicinity of the tunnel using a SD-like model. The decrement predicted by this model is 64.8% of the 2021 value. At increasing distances, the SD solution provides overestimations with respect to both 2012 and 2021 of about 123.3% and 133.3% in P1 and P2. In P3, SD returns to predict slight smaller values. Similar patterns can be identified for the PGA. Smaller differences are predicted at a depth of 3.0 m from ground (Fig. 15) between the various models, with the SD scenario that typically overestimates the predicted vibrations almost everywhere.

The previous quantities have been intensively used to provide a measure of the severity of human vibration exposure [49]. For the same purpose, acceleration-weighted levels can be calculated as well [33]. An appropriate filtering is always performed for two main reasons:

1. the effects of vibrations of different frequencies are cumulative;
2. vibrations are perceived differently depending on the frequency.

For the sake of simplicity, the procedure indicated by [33] is followed. In view of the free-field simulated conditions, this may lead to a sufficiently reliable estimate of the vibration that might be felt in various cases.

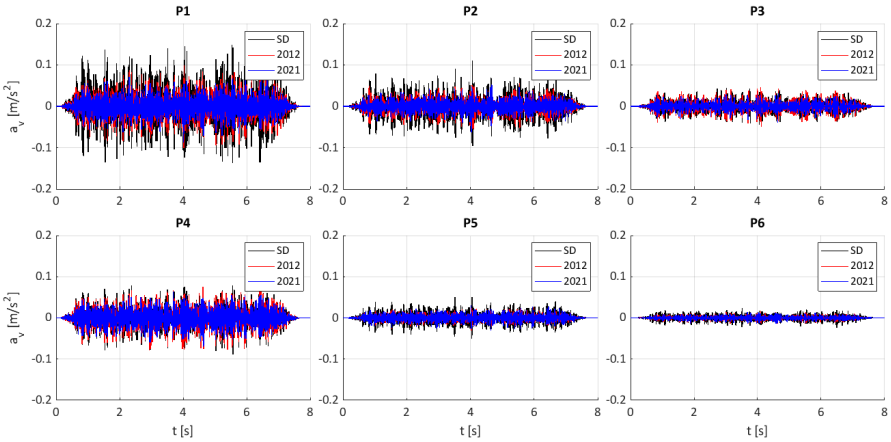

Figure 10: Time-histories of the vertical acceleration at control points P1, P2, P3, P4, P5 and P6 shown in Fig. 6.

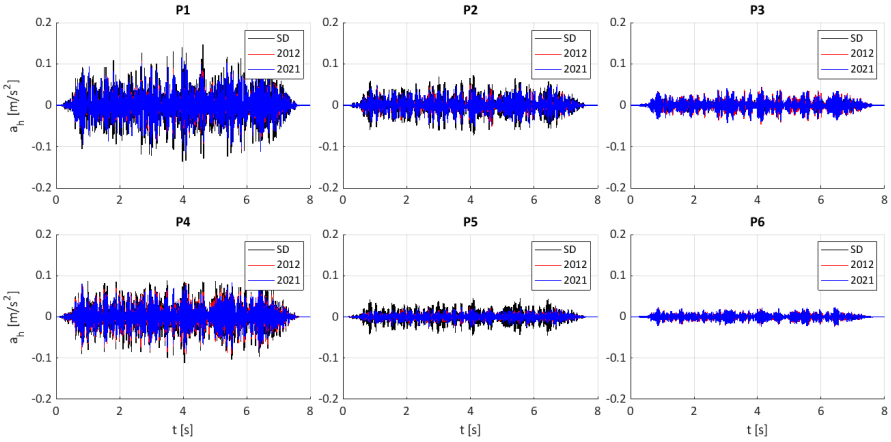

Figure 11: Time-histories of the horizontal acceleration at control points P1, P2, P3, P4, P5 and P6 shown in Fig. 6.

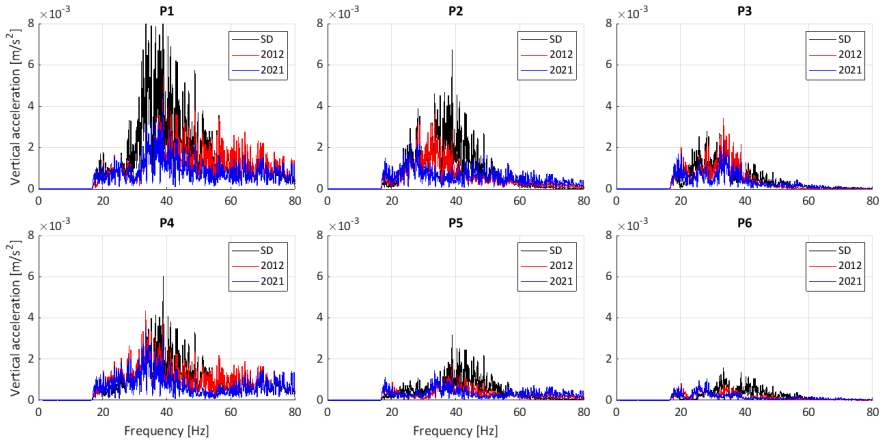

Figure 12: Fourier amplitude spectra of the vertical acceleration at control points P1, P2, P3, P4, P5 and P6 shown in Fig. 6.

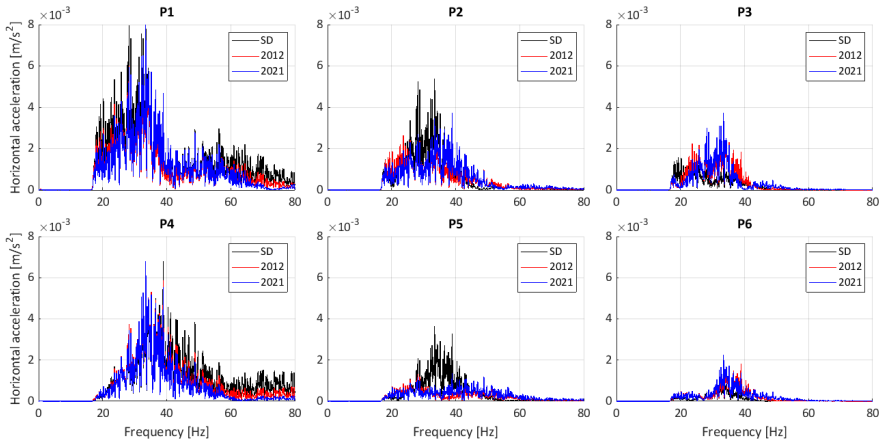

Figure 13: Fourier amplitude spectra of the horizontal acceleration at control points P1, P2, P3, P4, P5 and P6 shown in Fig. 6.

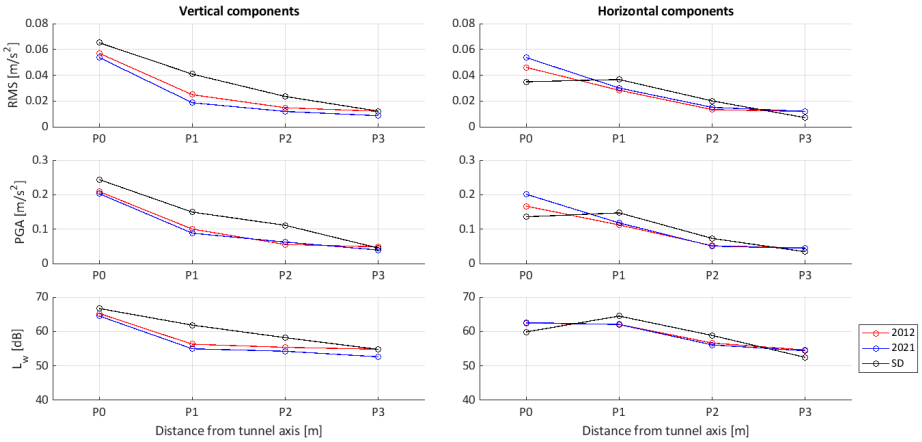

Figure 14: RMS, PGA and overall weighted acceleration level at control points P0, P1, P2 and P3 shown in Fig. 6.

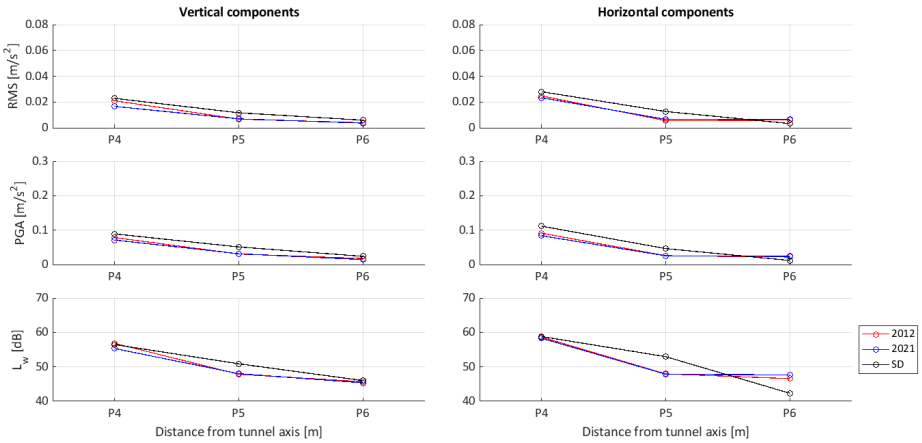

Figure 15: RMS, PGA and overall weighted acceleration level at control points P4, P5 and P6 shown in Fig. 6.

The acceleration level at the i-th thirds of octave band can be defined as:

$$L_i = 20Log\frac{a_i}{a_0} \tag{15}$$

being f_i the i-th central frequency and $a_0 = 10^{-6}\ m/s^2$ the reference acceleration. The weighted acceleration level is:

$$L_{w,i} = L_i - F_i \tag{16}$$

where F_i represents the attenuation defined by weighting filters for the i-th band. The filter used herein, referred to vibrations propagating along the axis passing through the human body back, provides an attenuation of 3.0 dB per band between 1.0 and 4.0 Hz, of 0.0 dB per band between 4.0 and 8.0 Hz and of 6.0 dB per band between 8.0 and 80.0 Hz. The overall acceleration-weighted level is finally computed as:

$$L_w = 10Log\sum_i 10^{L_{w,i}/10} \tag{17}$$

being the summation extended on all the thirds of octaves bands between 1 and 80 Hz. Results are reported in Fig. 14 and Fig. 15 together with RMS and PGA values at increasing distances from the tunnel. Small differences can be appreciated between the 2012 and 2021 at almost all the investigated depths. The SD scenario is confirmed to return overestimated overall weighted acceleration levels, with variations up to 6.8 dB for vertical accelerations and 2.0 dB for horizontal accelerations on surface (Fig. 14). A difference of 2.5 dB must be highlighted in P1, where the SD prediction returns smaller values. Small variations are observed at a depth of 3.0 m from the ground (Fig. 15). Anyway, in each situation the vibrations do not overcome the lowest critical values of 74.0 dB provided by [33]. The weighted acceleration which corresponds to the higher level, i.e. 66.7 dB for SD, is $2.2 \cdot 10^{-3}$ m/s^2, is still below the maximum allowable value of $5.0 \cdot 10^{-3}$ m/s^2. Such values may be amplified in the presence of structural elements in case of dynamic resonance.

The results shown provide a measure of the influence of different dynamic soil conditions on the propagation of vibrations induced by underground trains. The comparison between 2012 and 2021 scenarios highlight the temporal variation of the induced motion as the state of the soil changes, as suggested by the two different profiles determined by the geophysical tests. The

difference in the impedance distribution over depth returns changes between the two situations, even though the seasonal period and the water table location were similar, suggesting that the role played by shallower layers should be more thoroughly investigated for seasonal variations. Over-simplified assumption on the hydraulic and mechanical behaviour of the soil may lead to overly conservative estimates of the vibration levels, as shown by the SD model.

5. Discussion

The plane strain assumption implies that each vertical cross section is stressed by the same load at the same time. The approach enables the dynamic component to be superimposed on the distributed load coming from the static weight of the whole train, which is considered a more severe configuration for the system. Many numerical models used for the prediction of railway-induced vibrations are based on the decoupling shown in Eq. 7. As discussed in previous studies [3, 27], the effect of the static component of the axle load on the surroundings is highly dependent on the train speed, inducing increasing vibrations while approaching the critical phase velocity of the system, as it may happen for high speed trains running on soft soils. Since the trains of interest for this study move at much lower speeds, in the order of 50 km/h, the effect of the variation in time of the static load on the induced vibrations is assumed to be negligible. The adopted load (Eq. 7 and Fig. 9) aims to emphasize the role played only by the dynamic component.

To test the reliability of the models, including the latter assumption, results are checked against vibration measurements recently performed along the M1 metro line. Train passages were recorded for one hour with a sampling frequency of 1600 Hz by an accelerometer placed 1.5 m above the rail level in a tunnel similar to Fig. 1. Ten time-histories with appropriate duration were extracted using the Hanning window and analysed. The measures are compared with the computed ones in Fig. 16 in terms of Fourier amplitude spectra in thirds of octave bands. The agreement is judged to be good in view of the large amount of uncertainties affecting the comparison. Among them, a special mention is deserved by the load enforced in the FE model to represent the train. The type of convoy, track, rail track and tunnel as well as the velocity may differ from the one used in the definition of the reference spectrum used in this analysis. Therefore, imperfect matching of the simulations to measured signals is considered to be acceptable. All

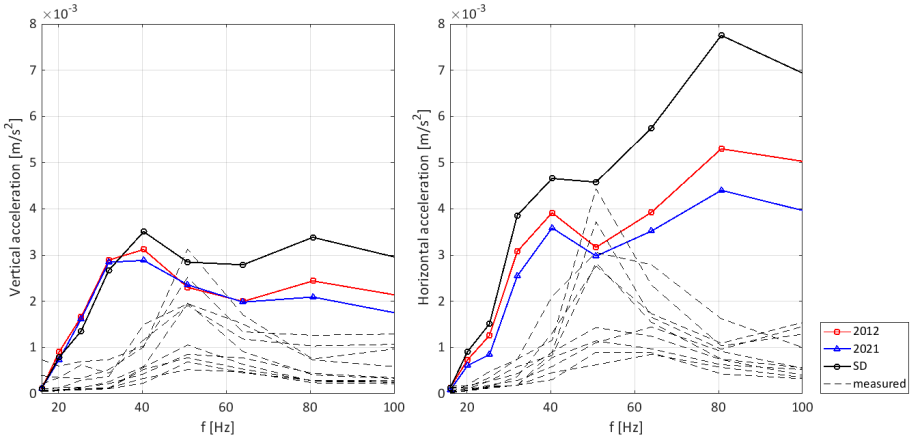

Figure 16: Comparison between measured and computed Fourier spectra.

the measures show a first peak at nearly 50 Hz, which may be related to the resonance frequency of the wheel-track system, which is independent of the train velocity. For higher frequencies, the computed signals show a higher energetic content, which is actually coherent with the shape of the load spectrum given as input (Fig. 9). Xu et al. (2016) [47] show how this part of the spectrum may be related to the presence of irregularities of small wavelength. Therefore, the shift of the peaks in the thirds of octave bands spectra between the calculated and measured signals can be attributed to different loading conditions. Furthermore, the comparison also suffers from the representation in frequency bands, which may result in a shift of peaks to adjacent bands. Nevertheless, in spite of the 2D approximation, the order of magnitude is rightly reproduced by the numerical models and the frequency range of interest is almost reconstructed. Discrepancies of the reconstructed signals may also derive from the assumption of plain strain which typically overestimates the vibrations with respect to 3D models [31]. Numerical or analytical methods which remove the 2D assumption [21, 26, 27] should be preferred if the problem being addressed is a reliable quantitative prediction of the vibration levels for design or mitigation purposes. For the case at hand, the expected discrepancy is deemed to be acceptable as the differences between two different dynamic conditions for the soil were to be investigated. The higher acceleration at the right tunnel wall is also due to the higher load used in the simulations, compared to the typical weight of the trains running on the specific line [33].

6. Conclusions

The contribution addresses the sensitivity of ground borne vibrations induced by underground trains to the dynamic state of the soil which may vary over seasons and years. The results of in-situ geophysical tests performed by MM at two different times on the same site in the centre of Milano were exploited to identify seasonal variations of the dynamic response of the site. Two-dimensional plane strain Finite Element models were set up, in an attempt to evaluate the role played by seasonal variations on the ground vibrations, coming from the unsaturated response of the soil layers above the water table. The models were excited by a synthetic load time history obtained by superposing the static load with a dynamic component obtained from a reference spectrum.

The proposed model shows that oversimplifying the numerical simulations, by assuming dry conditions above the water table, results in significant overestimation of the induced ground borne vibrations. Underestimations are also possible, especially in the vicinity of the tunnel. A more accurate profile of the relevant dynamic quantities as a function of the state of the soil allows reducing the artificial amplification of ground vibrations embedded in simpler models, and enables evaluating their seasonal variation, which is reported to affect human perception.

The reliability of the two dimensional model was checked against accelerations recorded on a tunnel wall on the underground infrastructure under analysis. Even though the artificial input used in the analyses could not match the unknown spectrum of the experimental load, neither the geometry correctly reproduced the full three-dimensional interaction problem, the results of the analyses show similar amplitudes for the most relevant low frequencies range, with the differences observed at higher frequencies highly dependent on the local imperfections of the train-track interaction.

To improve the current models, a 2.5D analysis is under development. Moreover, an investigation on the dynamic response of these soils at variable saturation has been undertaken.

The comparison of the results on two different profiles calibrated on in situ data collected in March 2012 and April 2021 showed few decibels difference, even though the seasonal period and the water table location were similar. The preliminary results demonstrate that, overall, variable seasonal conditions may have a role on the energy dissipation of ground borne vibrations, hence, on their perception at the ground surface. Also, they suggest that it

is worthwhile investigating more general climate scenarios, to evaluate the relative importance of this factor among those which can be responsible for variable vibrations perception over time, especially accounting for expected climatic stress changes.

References

[1] M. Heckl, G. Hauck, R. Wettschureck, Structure-borne sound and vibration from rail traffic, Journal of Sound and Vibration 193 (1) (1996) 175–184. doi:https://doi.org/10.1006/jsvi.1996.0257.

[2] D. Clouteau, G. Degrande, G. Lombaert, Numerical modelling of traffic induced vibrations, Meccanica 36 (4) (2001) 401–420.

[3] G. Lombaert, G. Degrande, Ground-borne vibration due to static and dynamic axle loads of intercity and high-speed trains, Journal of Sound and vibration 319 (3-5) (2009) 1036–1066.

[4] C. Esveld, C. Esveld, Modern railway track, Vol. 385, MRT-productions Zaltbommel, 2001.

[5] S. Gupta, Y. Stanus, G. Lombaert, G. Degrande, Influence of tunnel and soil parameters on vibrations from underground railways, Journal of Sound and Vibration 327 (1-2) (2009) 70–91.

[6] M. Schevenels, G. Degrandec, G. Lombaert, The influence of the depth of the ground water table on free field road traffic-induced vibrations, International journal for numerical and analytical methods in geomechanics 28 (5) (2004) 395–419.

[7] F. Rigoni, Effect of water table's depth in subway-induced vibrations: case of Line M1 in Milan, Ms's Diss, Politecnico di Milano, 2021.

[8] H. Di, S. Zhou, H. Guo, C. He, X. Zhang, Three-dimensional analytical model for vibrations from a tunnel embedded in an unsaturated half-space, Acta mechanica 232 (2021) 1543–1562.

[9] H. Di, H. Guo, S. Zhou, B. Wang, C. He, X. Zhang, An analytical model for evaluating the dynamic response of a tunnel embedded in layered foundation soil with different saturations, Earthquake Engineering and Engineering Vibration 21 (3) (2022) 663–681.

[10] W. Oh, S. Vanapalli, The relationship between the elastic and shear modulus of unsaturated soils, in: Proceedings of the 5th international conference on unsaturated soils, Barcelona, Spain, 2010, pp. 341–346.

[11] X. Qian, D. H. Gray, R. D. Woods, Voids and granulometry: effects on shear modulus of unsaturated sands, Journal of Geotechnical Engineering 119 (2) (1993) 295–314.

[12] R. Vassallo, C. Mancuso, F. Vinale, Effects of net stress and suction history on the small strain stiffness of a compacted clayey silt, Canadian geotechnical journal 44 (4) (2007) 447–462.

[13] R. Vassallo, C. Mancuso, F. Vinale, Modelling the influence of stress–strain history on the initial shear stiffness of an unsaturated compacted silt, Canadian Geotechnical Journal 44 (4) (2007) 463–472.

[14] C. Mancuso, R. Vassallo, A. d'Onofrio, Small strain behavior of a silty sand in controlled-suction resonant column torsional shear tests, Canadian Geotechnical Journal 39 (1) (2002) 22–31.

[15] A. Khosravi, P. Shahbazan, A. Pak, Impact of hydraulic hysteresis on the small strain shear modulus of unsaturated sand, Soils and Foundations 58 (2) (2018) 344–354.

[16] A. G. Pagano, A. Tarantino, V. Magnanimo, A microscale-based model for small-strain stiffness in unsaturated granular geomaterials, Géotechnique 69 (8) (2019) 687–700.

[17] M. Biglari, I. Ashayeri, An empirical model for shear modulus and damping ratio of unsaturated soils, in: Proc. 5th Asia-Pacific Conf. On Unsaturated Soils, Pataya, Thailand, 2012, pp. 591–596.

[18] I. Ishibashi, X. Zhang, Unified dynamic shear moduli and damping ratios of sand and clay, Soils and foundations 33 (1) (1993) 182–191.

[19] S. Foti, R. Lancellotta, L. V. Socco, L. Sambuelli, Application of fk analysis of surface waves for geotechnical characterization (2001).

[20] S. Foti, L. Sambuelli, V. L. Socco, C. Strobbia, Experiments of joint acquisition of seismic refraction and surface wave data, Near surface geophysics 1 (3) (2003) 119–129.

[21] J. Forrest, H. Hunt, A three-dimensional tunnel model for calculation of train-induced ground vibration, Journal of Sound and Vibration 294 (4) (2006) 678–705. doi:https://doi.org/10.1016/j.jsv.2005.12.032.

[22] T. Real, C. Zamorano, F. Ribes, J. Real, Train-induced vibration prediction in tunnels using 2d and 3d fem models in time domain, Tunnelling and Underground Space Technology 49 (2015) 376–383.

[23] X. Sheng, C. Jones, D. Thompson, Modelling ground vibration from railways using wavenumber finite-and boundary-element methods, Proceedings of the Royal Society A: Mathematical, Physical and Engineering Sciences 461 (2059) (2005) 2043–2070.

[24] Y.-B. Yang, H. Hung, Soil vibrations caused by underground moving trains, Journal of Geotechnical and Geoenvironmental Engineering 134 (11) (2008) 1633–1644.

[25] C. He, S. Zhou, H. Di, Y. Shan, A 2.5-d coupled fe–be model for the dynamic interaction between saturated soil and longitudinally invariant structures, Computers and Geotechnics 82 (2017) 211–222.

[26] S. Zhou, C. He, P. Guo, F. Yu, Dynamic response of a segmented tunnel in saturated soil using a 2.5-d fe-be methodology, Soil Dynamics and Earthquake Engineering 120 (2019) 386–397.

[27] S. Zhou, C. He, H. Di, P. Guo, X. Zhang, An efficient method for predicting train-induced vibrations from a tunnel in a poroelastic half-space, Engineering Analysis with Boundary Elements 85 (2017) 43–56.

[28] T. Balendra, K. Chua, K. Lo, S. Lee, Steady-state vibration of subway-soil-building system, Journal of engineering mechanics 115 (1) (1989) 145–162.

[29] K. Chua, K. Lo, T. Balendra, Building response due to subway train traffic, Journal of Geotechnical Engineering 121 (11) (1995) 747–754.

[30] L. Andersen, C. Jones, Coupled boundary and finite element analysis of vibration from railway tunnels—a comparison of two-and three-dimensional models, Journal of sound and vibration 293 (3-5) (2006) 611–625.

[31] Y. Yang, X. Liang, H.-H. Hung, Y. Wu, Comparative study of 2d and 2.5 d responses of long underground tunnels to moving train loads, Soil Dynamics and Earthquake Engineering 97 (2017) 86–100.

[32] Vibrazioni - Valutazione del comportamento statico e dinamico di sistemi di armamento ferrotranviario - Parte 1: Informazioni generali (UNI11389), Standard, Ente nazionale italiano di normazione, Milano, IT (Feb 2011).

[33] Misura delle vibrazioni negli edifici e criteri di valutazione del disturbo (UNI9614), Standard, Ente nazionale italiano di normazione, Milano, IT (Mar 1990).

[34] D. Rodemann, Tochnog professional user's manual (2022).

[35] D. P. Connolly, G. Kouroussis, O. Laghrouche, C. Ho, M. Forde, Benchmarking railway vibrations–track, vehicle, ground and building effects, Construction and Building Materials 92 (2015) 64–81.

[36] C. Niccolai, Il sottosuolo del territorio di milano, Rivista Italiana di Geotecnica 1 (1967) 7–33.

[37] T. Bonomi, Groundwater level evolution in the milan area: natural and human issues, IAHS PUBLICATION (1999) 195–202.

[38] F. E. Richart, J. R. Hall, R. D. Woods, Vibrations of soils and foundations, 1970.

[39] S. Nazarian, K. H. Stokoe II, W. R. Hudson, Use of spectral analysis of surface waves method for determination of moduli and thicknesses of pavement systems (930) (1983).

[40] J. N. Louie, Faster, better: shear-wave velocity to 100 meters depth from refraction microtremor arrays, Bulletin of the Seismological Society of America 91 (2) (2001) 347–364.

[41] Y. Nakamura, A method for dynamic characteristics estimation of subsurface using microtremor on the ground surface, Railway Technical Research Institute, Quarterly Reports 30 (1) (1989).

[42] O. C. Zienkiewicz, A. Chan, M. Pastor, B. Schrefler, T. Shiomi, Computational geomechanics, Vol. 613, Citeseer, 1999.

[43] D.M. 17 Gennaio 2018, Regulation, Ministero delle infrastrutture e dei trasporti, Roma, IT (Jan 2018).

[44] Legno strutturale - Classi di resistenza (UNIEN338), Standard, Ente nazionale italiano di normazione, Milano, IT (May 2016).

[45] K. T. Nguyen, D. S. Kusanovic, D. Asimaki, Dynamic soil impedance functions for cylindrical structures buried in elastic half-space, Soil Dynamics and Earthquake Engineering 162 (2022) 107431.

[46] J. Lysmer, R. L. Kuhlemeyer, Finite dynamic model for infinite media, Journal of the engineering mechanics division 95 (4) (1969) 859–877.

[47] Q.-y. Xu, X. Ou, F. Au, P. Lou, Z.-c. Xiao, Effects of track irregularities on environmental vibration caused by underground railway, European Journal of Mechanics-A/Solids 59 (2016) 280–293.

[48] E. Vanmarcke, D. Gasparini, Simulated earthquake ground motions (1977).

[49] M. J. Griffin, J. Erdreich, Handbook of human vibration (1991).